International Journal of Nanomedicine

Dovepress
open access to scientific and medical research

Open Access Full Text Article

ORIGINAL RESEARCH

NIR-guided dendritic nanoplatform for improving antitumor efficacy by combining chemo-phototherapy

This article was published in the following Dove Press journal:
International Journal of Nanomedicine

Ruifen Ge[1,*]
Jie Cao[1,*]
Jinnan Chi[1]
Shangcong Han[1]
Yan Liang[1]
Lisa Xu[1]
Mingtao Liang[2]
Yong Sun[1]

[1]Department of Pharmaceutics, School of Pharmacy, Qingdao University, Qingdao, People's Republic of China; [2]Department of Pharmaceutics, School of Biomedical Science and Pharmacy, University of Newcastle, Newcastle, New South Wales, Australia

*These authors contributed equally to this work

Background: Phototherapy, including photothermal therapy (PTT) and photodynamic therapy (PDT), is a promising noninvasive strategy in the treatment of cancers due to its highly localized specificity to tumors and minimal side effects to normal tissues. However, single phototherapy often causes tumor recurrence which hinders its clinical applications. Therefore, developing a NIR-guided dendritic nanoplatform for improving the phototherapy effect and reducing the recurrence of tumors by synergistic chemotherapy and phototherapy is essential.

Methods: A fluorescent targeting ligand, insisting of ICG derivative cypate and a tumor penetration peptide iRGD (CRGDKGPDC), was covalently combined with PAMAM dendrimer to prepare a single agent-based dendritic theranostic nanoplatform iRGD-cypate-PAMAM-DTX (RCPD).

Results: Compared with free cypate, the resulted RCPD could generate enhanced singlet oxygen species while maintaining its fluorescence intensity and heat generation ability when subjected to NIR irradiation. Furthermore, our in vitro and in vivo therapeutic studies demonstrated that compared with phototherapy or chemotherapy alone, the combinatorial chemo-photo treatment of RCPD with the local exposure of NIR light can significantly improve anti-tumor efficiency and reduce the risk of recurrence of tumors.

Conclusion: The multifunctional theranostic platform (RCPD) could be used as a promising method for NIR fluorescence image-guided combinatorial treatment of tumor cancers.

Keywords: phototherapy, chemotherapy, combined therapy, dendrimer, ICG derivatives

Introduction

Phototherapy on cancer treatment has attracted increasing interests on cancer treatment for its simplicity, high efficiency, high selectivity to tumor tissue, and minimal trauma to normal tissue. Phototherapy contains two major species, photodynamic therapy (PDT) and photothermal therapy (PTT).[1–6] Specifically, PDT is a phototoxic therapy wherein the photosensitizer is excited with light of a specific wavelength to generate singlet oxygen ($^1O_2$) and other reactive oxygen species (ROS) that can produce light toxic effects.[7] PTT takes advantage of photothermic agents to absorb lights at certain wavelengths, and then transform it to heat at tumor site, thereby killing cancer cells via hyperthermia or thermal ablation.[8] However, phototherapy alone cannot kill cancer cells entirely due to the uneven heat distribution and hypoxic condition within the tumor.[9] It can only cure early tumors and small lesions, but for advanced cancers, phototherapy alone could cause local

Correspondence: Yong Sun
Department of Pharmaceutics, School of Pharmacy, Qingdao University, 38 Dengzhou Road, Qingdao 266021, People's Republic of China
Tel +86 5 328 299 1203
Email sunyong@qdu.edu.cn

submit your manuscript | www.dovepress.com
DovePress
http://doi.org/10.2147/IJN.S203171

recurrence and distant metastasis.[10,11] To overcome these drawbacks and enhance antitumor efficiency, the use of comprehensive treatment composed of different methods has become a new trend in cancer treatment. Recently, synergistic chemo-phototherapy has demonstrated its abilities to enhance therapeutic efficacies and reduce undesired side effects in pre-clinical animal studies, and shown unique advantages compared with conventional chemotherapy.[9,12] The mechanisms of combined treatment of chemo-phototherapy are complicated. Apart from the direct sum of damages caused by both modalities, the resultant effects on the tumor vasculature and the induction of immune responses all contribute to the anticancer effects of chemo-phototherapy. In particular, phototherapy could permeabilize tumor vasculature, which may result in enhanced drug delivery; moreover, chemotherapy can enhance the efficacy of phototherapy by targeting surviving cancer cells or by inhibiting regrowth of damaged tumor blood vessels.[9] Meanwhile, ROS and local hyperthermia generated by phototherapy would activate cancer cells sensitive to the chemotherapy drugs.[13,14]

Recently, several multifunctional theranostic systems have been developed for achieving combinatorial chemo-phototherapeutic treatment of cancer.[15–23] NIR light lies in the "optical transparency window" of biological tissues due to its low autofluorescence and reduced light scattering, which promotes deeper penetration and reduced phototoxicity to live organisms.[24–26] Hence, PDT and PTT agents exhibited strong absorbance in the near infrared (NIR) region (700–1000 nm) are essential for achieving chemo-phototherapy. The main approach for construction of these systems is based on the integration of separate PDT agents and PTT agents into nanocarriers, which results in complex theranostic systems with limited translational potentials.[27–29] Thus, there is a desire to develop single agent-based nanoparticles for synergistic chemo and phototherapy, which can simultaneously exhibit strong PDT efficacy during its PTT process. ICG, a FDA approved and clinically used NIR cyanine dye, may be a good candidate for this criterion. Since ICG or ICG derivatives are known to exhibit both PDT and PTT effects, and could exhibit strong absorbance in NIR region, tremendous studies have been reported using ICG or ICG derivatives for combined anticancer chemo-phototherapy.[30–44] However, most of the reports focused on the combination of only part function of phototherapy (PDT or PTT only) with chemotherapy, which may reduce the resultant therapeutic effects.[30–36] For the studies of combined phototherapy (PDT+PTT) with chemotherapy, the NIR dyes were usually encapsulated in the nanocarriers, which could reduce the PDT effect due to the self-aggregation of NIR dyes.[37–41] Miao et al prepared photo-decomposable nanoparticles by covalently binding ICG derivative cypate to PEG.[45] Although the nanoparticles were not used for synergistic chemo-phototherapy, the self-assembly PEGylated cypate exhibited enhanced PDT effect compared with free cypate, which motivated us to use our previously reported triplet modality dendritic nanoplatform (iRGD-cypate-PAMAM, RCP) for enhanced combination of chemo- and photo-therapy. RCP combined a hydrophobic cyanine dye cypate with dendrimer (PAMAM) and modified with a tumor penetration peptide iRGD to improve hydrophilicity and reduce the self-aggregation of cypate.[46] We speculate that the dispersion of cypate onto the outer space of dendrimers would reduce the self-quenching of cypate, therefore increase its fluorescence intensity and PDT effect. Hence, in this paper, we mainly focus on the ROS and heat generation of RCP to investigate its PDT and PTT effects. Besides, to reduce the tumor recurrence, a broad-spectrum chemotherapeutic drug DTX (Docetaxel) was encapsulated into the inner space of RCP that can combine chemotherapy with phototherapy and alleviate adverse effects of DTX by improving its in vitro and in vivo stabilities. Based on the above-mentioned design and mechanism, we hypothesized that this multi-mechanism theranostic platform could reduce the recurrence rate of cancer and enhance anti-tumor efficiency.

Materials and methods

Materials

PAMAM dendrimer (ethylenediamine core, G5), 2′,7′-dichlorodihy drofluorescein diacetate (DCFH-DA), docetaxel (DTX), 1-ethyl-3-(3′-dimethylaminopropyl) carbodiimide (EDC), N-hydroxysuccinimide (NHS), 1,3-Diphenylisobenzofuran (DPBF) were all purchased from Sigma-Aldrich (St. Louis, USA). Indocyanine Green (ICG) derivative Cypate (MW 627.32) was prepared in our laboratory and iRGD was purchased from Shanghai GL Biochem. Singlet Oxygen Sensor Green (SOSG) was purchased from Invitrogen-Life Technologies (Carlsbad, CA, USA). Methyl thiazolyltetrazolium (MTT), Lysotracker Green, Calcein AM/PI assay kit, Annexin V-FITC/PI apoptosis staining kit were purchased from Solarbio (Beijing, China). All other analytical reagent grade chemical reagents used in the study

were commercially acquired from Shanghai Chemical Reagent Company (Shanghai, China). Human liver cancer cell (HepG2) was purchased from American Type Culture Collection (ATCC, Manassas, VA, USA). Cells were cultured in Dulbecco's Modified Eagle Medium (DMEM, Sigma, USA) supplemented with 10% fetal bovine serum (Solarbio, Beijing, China) and 1% penicillin–streptomycin (Solarbio, Beijing, China). Cells were grown at 37°C under a humidified atmosphere of 5% CO_2 (v/v) in air. A DTX-resistant human liver cancer cell (HepG2) was obtained by cultivating human liver cancer cell (HepG2) cells in DMEM supplemented with 10% of FBS and intermittent low and increasing DTX concentrations (2−10 mg/L). The athymic nude mice (nu/nu CD-1) (half male and half female) used in this study were purchased from Daren Laboratory Animal Co. Ltd. (Qingdao, China), which were 6–8 weeks old and weighed about 18–22 g. All animal experiments were carried out in compliance with the Animal Management Rules of the Ministry of Health of the People's Republic of China (document no. 55, 2001) and were approved by the Animal Care Ethics Committee of Qingdao University (Qingdao, China).

Preparation of the theranostic nanoplatform

iRGD-cypate-PAMAM-DTX (RCPD) was synthesized according to our previous report.[46] In brief, iRGD-cypate was firstly synthesized by amide reaction of cypate and iRGD peptide. Then the –COOH of iRGD-cypate with NHS/EDC system in DMF (molar ratio of iRGD-cypate: NHS: EDC=1:1.5:1.5) was activated for 30 mins; and reacted with 0.2 mmol dendrimer G5 in pH 6.0 PBS overnight at room temperature. The product was purified by dialysis (MWCO10000) for 1–2 d against pH 6.0 PBS to remove the unreacted reagents, and then centrifuged to remove unreacted iRGD-cypate.

iRGD-cypate-PAMAM-DTX (RCPD) was prepared by adding methanol solution of DTX to an equal volume of RCP in PBS (molar ratio of DTX: RCPD=10:1), and stirred for 24 hrs at room temperature. Then the product was purified by dialysis (MWCO10000) for 1–2 d against pH 7.4 PBS to remove the unreacted reagents and collected by centrifugation. The supernatant liquid was collected to determinate the drug loading efficiency by HPLC. The amount of encapsulated DTX was determined by subtracting the remnant DTX in the supernatant liquid after drug loading from the initial amount of DTX was added.

Characterization of the theranostic nanoplatform

The absorption and fluorescence spectra of RCPD in PBS buffer were measured using Beckman Coulter DU 640 spectrophotometers and Fluorolog-3 fluorometer, respectively. All optical measurements were performed at room temperature. The hydrodynamic size and zeta potential of prepared complexes were measured by Mastersizer Nano-ZS90 laser particle size analyzer (Malvern, UK). All measurements were performed at 25°C after pre-equilibration for 2 mins and each parameter was measured in triplicate. The morphologies of RCPD were observed by TEM (JEOL, JEM-1200EX).

In vitro PDT and PTT evaluation of RCPD

SOSG is used to detect $^1O_2$ generation after laser irradiation. SOSG is a specific fluorescence probe for detection of $^1O_2$, which could emit green fluorescence in the presence of singlet oxygen (excitation/emission max ~504/525 nm). Firstly, 50 μL of the 25 μM stock solution of SOSG in methanol and 150 μL of RCPD (0.02–0.16 mM cypate-equiv.) or cypate (0.16 mM) in PBS (pH=7.4) were added to the parallel wells. Next, all wells were irradiated with NIR light at different power density for different time (808 nm, 0.3, 0.96, or 1.6 W/cm^2, 1–7 mins), while PBS with or without NIR irradiation was as control. All the samples were immediately analyzed with Flex Station 3 (Molecular Devices) using an excitation of 504 nm and an emission of 525 nm.

Singlet oxygen quantum yield (Φ_Δ) of cypate and RCPD were calculated as Equation $\Phi_{\Delta\ (T)}=\Phi_{\Delta\ (MB)}\ (S_T/S_{MB})\ (F_{MB}/F_T)$,[47] where $\Phi_{\Delta(MB)}$ is the singlet oxygen quantum yield for the standard methylene blue (MB, $\Phi_{\Delta(MB)}$=0.52), "S" is the rate of light absorption of DPBF at 410 nm in the presence of samples and the standard upon irradiation, "F" is the absorption correction factor of samples and the standard, respectively. $F=1\text{-}10^{-OD}$, where OD represents the absorption value of samples and the standard at irradiation wavelength. To avoid chain reactions induced by quenchers (DPBF) in the presence of singlet oxygen, the concentration of quencher (DPBF) was lowered than 3×10^{-5} M. The subscripts "T" and "MB" represent the sample and the standard, respectively.

An 808-nm laser device (CL808-20-F, Photons Co Ltd) was employed. To evaluate the laser-induced temperature increase, ① 200 μL of RCPD aqueous solution (0.02–0.16 mM cypate-equiv.) was added into parallel wells of 96-well opaque plate. Then each well was irradiated with

laser (1.6 W/cm^2) for 6 mins; ② 200 μL of RCPD aqueous solution (0.16 mM cypate-equiv.) was added into parallel wells of 96-well opaque plate, and then each well was irradiated with laser in different power density (0.3, 0.96, or 1.6 W/cm^2) for 6 mins; ③ 200 μL of RCPD (0.16 mM cypate-equiv.) or cypate (0.16 mM) was added into parallel wells of 96-well opaque plate, and then each well was irradiated with laser (1.6 W/cm^2) for 10 mins. Temperature was monitored with a thermocouple thermometer (TES Electrical Electronic Corp, WRNK-104) at designated time intervals.

In vitro drug release study

In vitro drug release profile was studied using a dialysis method in PBS (pH 7.4 and 5.5). In brief, RCPD (equivalent to 400 μg of DTX) or PAMAM@DTX (equivalent to 400 μg of DTX) and DTX suspension (400 μg) were placed in dialysis tubing (MWCO 10000) in release medium (25 mL of PBS) at 37°C and stirred at 100 rpm. At different time intervals, 1 mL solution was withdrawn from released medium and replaced with the same volume of fresh medium. The samples were diluted, filtered through a 0.22 μm nylon filter, and analyzed by HPLC. The drug encapsulation efficiency (EE=(mass of drug loaded in dendrimers/mass of drug fed initially)×100%) and drug loading content (DLC=(mass of drug loaded in dendrimers/mass of drug-loaded dendrimers) ×100%) were analyzed by HPLC (Agilent 1260, USA). Each sample was analyzed in triplicate.

Cellular uptakes and intracellular locations

Cellular uptakes and intracellular locations of RCPD in HepG2 cells were studied by confocal microscopy. Cells were seeded onto confocal petri dish at a density of 1×10^5 cells/mL and incubated at 37°C for 12 hrs. 200 μL of RCPD aqueous solution (32 μM cypate-equiv.) was added into cell culture media. After incubation for 1 hr, 2 hrs, 4 hrs, 12 hrs, cells were washed with cold PBS, fixed with 4% paraformaldehyde for 15 mins, and stained with Lysotracker Green. Cellular fluorescence was observed using a confocal laser-scanning microscope (Nikon A1R MP, Japan).

Evaluation of PTT/PDT efficacies of RCPD in cancer cells

Photothermal efficacy of RCPD was evaluated in HepG2 cells. Briefly, cells were seeded into 6-well plates with a density of 1.5×10^6 cells/well and cultured for 24 hrs. After that, the culture media were replaced with fresh culture media containing free cypate or RCPD at a cypate concentration of 32 μM. After further incubation for 2 hrs, 1×10^6 cells were collected, suspended in 100 μL PBS, and then treated with laser irradiation at a power density of 0.3 W/cm^2 or 1.6 W/cm^2 for 5 mins. During laser irradiation, the temperatures of these cells were monitored every 30 seconds using a thermocouple thermometer.

To evaluate the photodynamic efficacy of RCPD, we detected ROS production in HepG2 cells after treatment using 2′,7′-dichlorofluorescin diacetate (DCFH-DA) as a fluorescence probe. In detail, HepG2 cells were seeded onto confocal petri dish at a density of 1×10^5 cells per well. After 24 hrs incubation, cells were treated with cypate or RCPD at a cypate concentration of 32 μM for 2 hrs. After washing with cold PBS, cells were irradiated with a NIR laser (808 nm, 0.3 W/cm^2 or 1.6 W/cm^2) for 5 mins and then incubated with fresh media containing DCFH-DA (10 μM) for 30 mins. In parallel, cells without NIR dyes were considered as a control. Finally, cells were imaged by laser scanning confocal microscopy and quantitative analysis by flow cytometry.

In vitro combination therapeutic efficacy and cell apoptosis analysis

Synergistic cytotoxicity of PTT/PDT and chemotherapy mediated by RCPD was assessed in DTX-resistant human liver cancer cells by MTT assay. Briefly, cells were seeded into 96-well plates at a density of 1×10^4 cells/well and incubated with culture medium, free DTX, RCP, and RCPD for 2 hrs. After washing with cold PBS, cells were irradiated with an 808-nm laser at designed power density for 5 mins and incubated for another 24 hrs. Then cells were processed with MTT and the absorbance of each well was detected by a microplate reader (Biorad, USA) at 490 nm. Meanwhile, cytotoxicity of RCP and RCPD in DTX-resistant human liver cancer cells and HepG2 cells at 24 hrs and 48 hrs were also detected.

Synergistic PDT/PTT-chemotherapy effects of RCPD on HepG2 cells were further verified using Calcein AM and propidium iodide (PI) co-staining. Briefly, HepG2 cells were incubated with culture medium, free DTX, cypate, RCP, and RCPD, and then irradiated at a power density of 0.3 W/cm^2 or 1.6 W/cm^2 for 5 mins. After laser irradiation, cells were incubated for another 24 hrs and stained with a mixed solution of calcein AM and PI at room temperature for 15 mins, followed by washing with PBS for thrice. The stained cells were examined under laser scanning confocal microscopy. Excitation

wavelength was set at 490 nm for calcein AM and 535 nm for PI.

Cell apoptosis was detected in HepG2 cells by the flow cytometry to further study synergistic effect of PTT/PDT and chemotherapy of RCPD. Briefly, cells were seeded in 6-well plates at a density of 3×10^5 cells/well and incubated with culture medium, free DTX, cypate, RCP, and RCPD. Some samples were irradiated at a power density of 0.3 W/cm^2 or 1.6 W/cm^2 for 5 mins. After further incubation for 24 hrs, all cells were processed with Annexin V-FITC apoptosis detection kit (Solarbio, China) in accordance with the manufacturer's protocol and finally analyzed by a flow cytometry.

In vivo PDT/PTT efficacy of RCPD

Athymic nude mice (half male and half female) were subcutaneously inoculated in the dorsal left side with 1×10^7 HepG2 cells, and tumors were allowed to become established over time. For evaluation of PTT efficacy, HepG2 tumor-bearing mice were intravenous injected separately with normal saline (as the control group), RCP and RCPD at the cypate and DTX dose of 6.7 and 5 mg/kg. After 24 hrs, tumors in these mice were exposed to an 808-nm laser at a power density of 0.3 W/cm^2 and 1.6 W/cm^2 for 5 mins. During the laser irradiation, temperature changes were recorded every 30 seconds by a thermocouple thermometer. For evaluation of PDT efficacy, SOSG was used as a fluorescence probe to detect intratumoral $^1O_2$ production. Briefly, 200 μL of normal saline, free DTX, RCP, and RCPD were injected into the vessel of mice. Then tumors were injected 50 μL SOSG (25 μM) and exposed to laser irradiation as above described after 24 hrs, all mice were sacrificed and tumors were collected for cryosection at 6 hrs after irradiation. Finally, tumor sections were visualized by a laser scanning confocal microscopy.

In vivo synergistic anticancer efficacy of RCPD

HepG2 tumor-bearing mice were randomly divided into seven groups with at least 5 mice each group and separately received treatments of normal saline, NIR light, free DTX, RCPD, RCP with laser irradiation (1.6 W/cm^2), RCPD with laser irradiation (0.3 W/cm^2 or 1.6 W/cm^2). All treatments were administered every 5 days via intravenous injection. cypate and DTX doses were 6.7 and 5 mg/kg, respectively. The laser irradiation was carried out on the tumors for 5 mins. The tumor volumes and body weights of these mice were measured every other day for 20 days. For histopathological examination, the aforementioned tumors were fixed in 4% paraformaldehyde, embedded in paraffin, and cut into 5-mm-thick sections. Finally, these sections were stained with H&E and imaged by a fluorescence microscope.

Statistical analysis

Data were analyzed using descriptive statistics, single-factor analysis of variance (ANOVA), and presented as mean values ± standard deviation (SD) from three to five independent measurements. The comparison among groups was performed by the independent sample Student's *t*-test. The differences were considered significant at a level of $P<0.05$.

Results and discussion

Synthesis and characterization of RCPD

It has been reported that hydrophobic free cypate could easily form H-aggregate, and subsequently cause strong intramolecular Förster resonance energy transfer (FRET) effect due to close proximity, which resulted in self-quenching and reducing $^1O_2$ generation.[46] Covalent of cypate onto the amino group of dendrimers may disperse the cypate moieties and reduce their self-quenching. Hence, in this study, we prepared a multifunctional nanoplatform iRGD-cypate-PAMAM-DTX (RCPD) to enhance PDT and achieve synergistic phototherapy and chemotherapy with increased cancer treatment capacity. The synthesis procedures of RCPD have been illustrated in Figure 1A. Particularly, cypate was firstly reacted with iRGD via amidation, and then the resulted iRGD-cypate was reacted with PAMAM by amide reaction to form RCP dendrimers. Finally, DTX was encapsulated into the inner core of RCP dendrimers. Absorption and fluorescence spectra of RCPD shown in Figure 1B showed that the absorption contained a monomer peak at 790 nm and a dimer peak at 730 nm, and the corresponding fluorescence spectra showed the maximum emission wavelength at 820 nm, which demonstrated that the resulted nanoplatform could be used for NIR imaging. Dynamic light scattering (DLS) measurements of RCP and RCPD showed a narrow size distribution with an average hydrodynamic diameter of 120.37±5.63 nm and 150.67±12.58 nm, respectively (Figures S1 and 1C), and the morphological characteristics of RCPD are a uniform spherical shape (Figure S2). Moreover, the zeta potential decreased to +5.02 mV

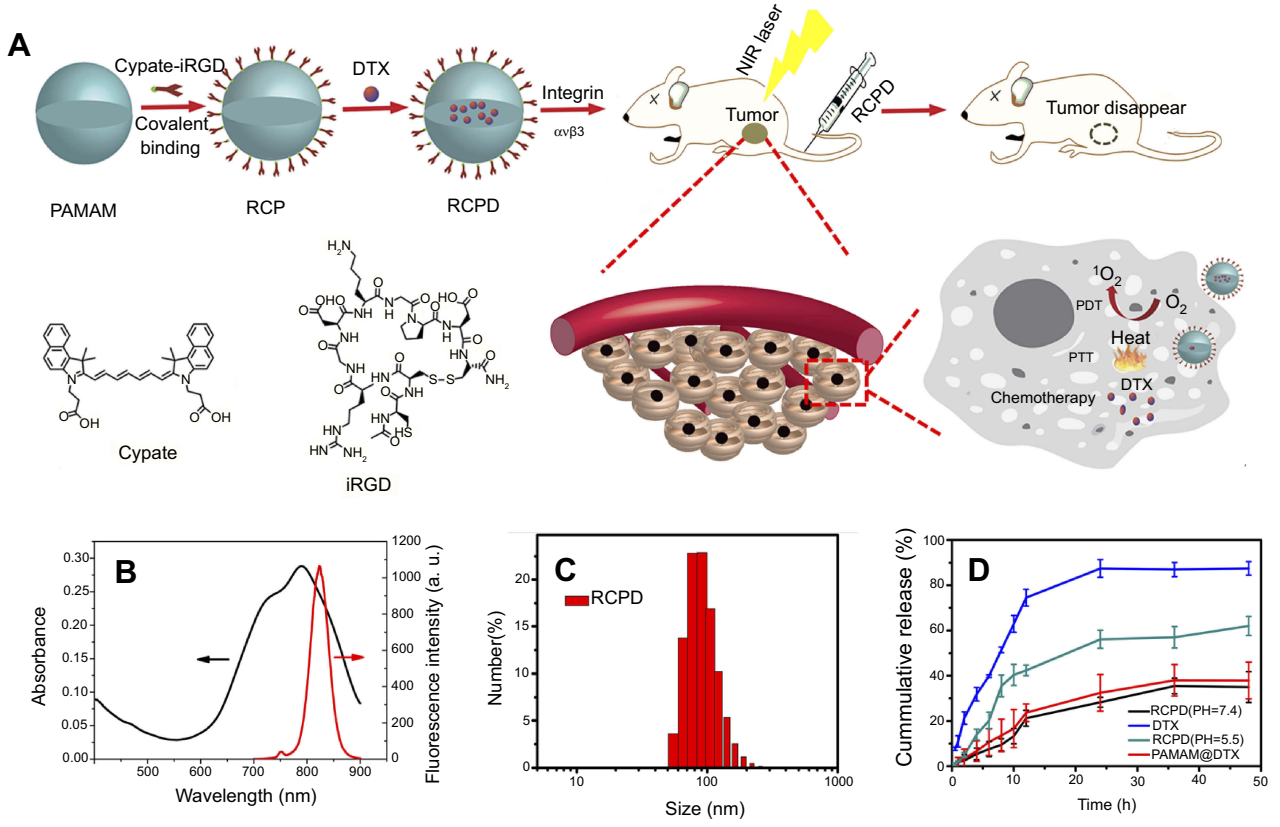

Figure 1 (**A**) Schematic representation of the synthesis of theranostic platform RCPD for combined chemo-photo treatment of cancer cells. (**B**) UV–Vis absorption and fluorescence spectra of RCPD. (**C**) Size distribution of RCPD. (**D**) Drug release profiles of DTX from DTX suspension, RCPD (pH=5.5 or 7.4), PAMAM@DTX.

(Figure S1) compared to non-modified PAMAM (+12.4 mV). The lower surface charge will reduce the interaction of the delivery system with macrophages during systemic circulation and decrease its toxicity related to cellular membrane damage effect.

To enable synergistic phototherapy and chemotherapy of RCPD, release profile of DTX was needed to be investigated first. The drug encapsulation efficiency and loading content of DTX were found to be approximately 27.8% and 5.91%, respectively. DTX released from RCPD was monitored in phosphate buffer saline (PBS with different pH). DTX suspension release was considered as control. As shown in Figure 1D, about 90.19% of DTX was released from DTX suspension within 24 hrs. In contrast, DTX was released from RCPD in a sustained manner under both pH5.5 and pH 7.4 conditions. Compared with PAMAM@DTX, the release of DTX from RCPD was much slower. For instance, 23.65% of DTX was released from PAMAM@DTX, while only 21.2% DTX from RCPD within 12 hrs. This may due to the presence of iRGD-cypate on the dendrimer surface, which could make a long release path for the drug or create a coat around the dendrimers that decreases diffusion of drug from dendrimers. In acetate buffer (pH 5.5), about 49.2% of drug was released from RCPD within 24 hrs, while only 26.71% of DTX was released in 24 hrs in PBS (pH 7.4). The difference between the releasing rates in the two buffers may attribute to the different degrees of protonation of the internal tertiary amine group of PAMAM under different pH conditions. Particularly, protonation of tertiary amine group of PAMAM is increased under acidic pH conditions, leading to the charge repulsion in the molecular chains of PAMAM and subsequently swell the PAMAM chains significantly. As a result, DTX can be released from the dendrimer interior in a faster manner. Additionally, the faster release in PBS (pH 5.5) is beneficial to the release of DTX in tumor tissues since the tumors hold the similar pH environment. Besides, the slow release of DTX in PBS (pH 7.4) demonstrated that the drugs could be well protected and premature drug leakage in blood circulation can be avoided.

In vitro photodynamic efficiency and photothermal efficiency

The ability to generate $^1O_2$ is an important indicator for evaluating photodynamic effect. Here, we examined the ability of RCPD to generate $^1O_2$ in response to NIR laser irradiation by measuring singlet oxygen quantum yield (Φ_Δ) and fluorescence intensity of SOSG. Cypate and RCPD were irradiated with a portable laser of power density at 1.6 W/cm^2 for 5 mins. PBS with the same irradiation was used as a control. As shown in Figure 2A, fluorescence intensity ratio of RCPD/PBS was higher (~2.85-fold) compared with cypate/PBS under NIR irradiation. Singlet oxygen quantum yield (Φ_Δ) of cypate and RCPD was calculated as 0.17 and 0.44 (~3.67-fold to ICG, ~2.59-fold to cypate) according to equation $\Phi_{\Delta\ (T)}=\Phi_{\Delta\ (MB)}\ (S_T/S_{MB})\ (F_{MB}/F_T)$.[47,48] These results demonstrated RCPD could enhance $^1O_2$ generation of cypate, indicating that the cypate moieties in RCPD were not close packed. In addition, $^1O_2$ is rapidly produced from RCPD in the beginning 1 min, and the generation rate maintained stable within 5 mins (Figure S3), indicating that enough ROS could be generated for PDT at 1–5 mins. By increasing the power density of NIR light and concentration of RCPD, $^1O_2$ generation was enhanced accordingly. As shown in Figure 2B and C, compared with 0.3 W/cm^2, the fluorescence intensity of SOSG is 3.21-fold higher when irradiated with NIR laser at 1.6 W/cm^2, and singlet oxygen production rose by 3.76 times with the concentration of RCPD increased from 0.02 mM to 0.16 mM (cypate-equiv). The reason was that the content of cypate and excited cypate was gradually increased with increasing concentration of RCPD and power density of NIR light. The abovementioned results indicated that RCPD showed distinctive singlet oxygen production which varied with power density and concentration.

To evaluate in vitro photothermal efficiency, cypate and RCPD were exposed to 808 nm laser at a power density of 1.6 W/cm^2; the temperature changes during the exposure were monitored and recorded. As shown in Figure 2D, the temperature profiles of both cypate and RCPD had a quick rising phase and reached a plateau at 75°C within 3 mins of irradiation. Temperature of cypate began to drop rapidly after 5 mins whereas the temperature of RCPD dropped slowly and stabled at about 66°C, which is due to the poor photostability of cypate and resulted in

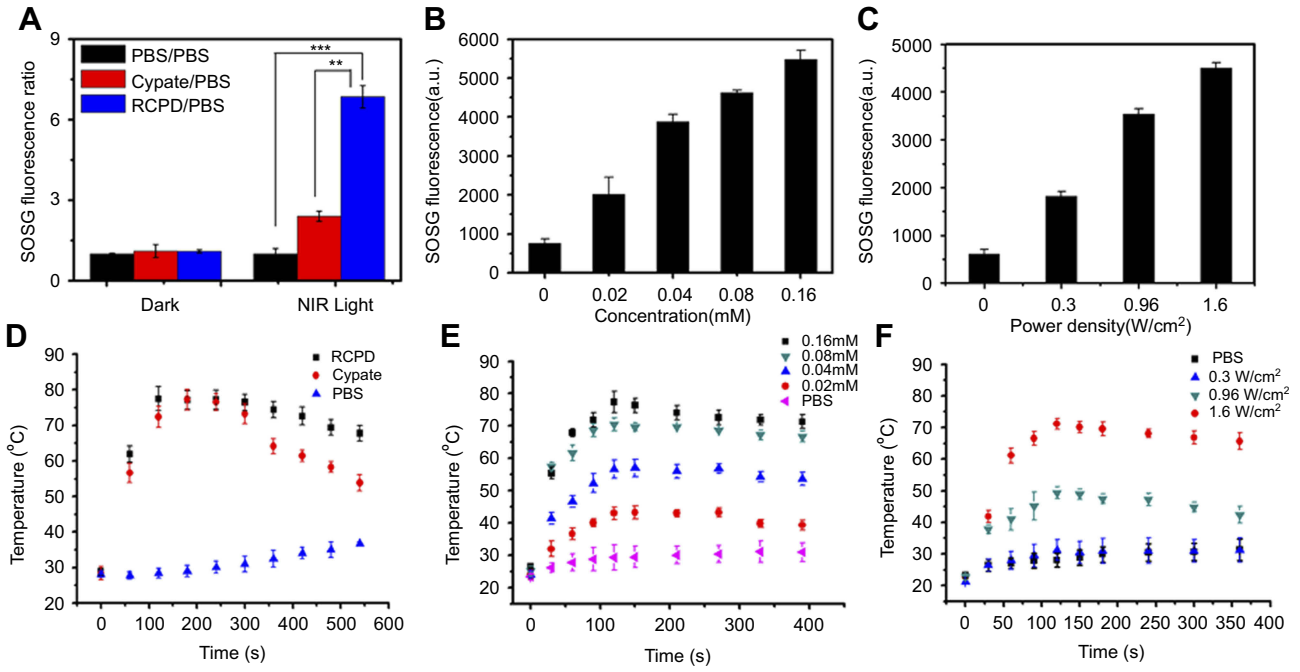

Figure 2 (**A**) Fluorescence intensity ratio of cypate and RCPD with PBS (0.16 mM cypate-equiv.) before (dark) and after (light) NIR irradiation (1.6 W/cm^2, 5 mins). **p<0.01, ***p<0.001. (**B**) Singlet oxygen generation by RCPD (0.02–0.16 mM cypate-equiv.) after NIR irradiation (1.6 W/cm^2, 5 mins). (**C**) Singlet oxygen generation by RCPD (0.16 mM cypate-equiv.) after NIR irradiation with different power density (0.3, 0.96, 1.6 W/cm^2, 5 mins). (**D**) Temperature change curves of PBS, cypate, and RCPD aqueous solution (0.16 mM cypate-equiv.) exposed to laser at a power density of 1.6 W/cm^2. (**E**) Temperature change curves of RCPD aqueous solution (0.02–0.16 mM cypate-equiv.) exposed to laser at a power density of 1.6 W/cm^2. (**F**) Temperature change curves of RCPD aqueous solution (0.16 mM cypate-equiv.) exposed to laser at the following power densities: 0.3, 0.96 and 1.6 W/cm^2.

photobleaching when exposed to NIR light.[50] While under the same conditions, the PBS control showed a temperature increase of only 8.5°C. The results showed that RCPD had the potential to first raise the temperature and then maintain the elevated temperature at cancer site. Further experiments were carried out by varying the concentration of RCPD and laser densities (from 0.3 to 1.6 W/cm^2). As shown in Figure 2E, higher concentrations of RCPD resulted in faster temperature elevations and higher temperature values. When the power density of the laser beam was lowered to 0.3 W/cm^2, no obvious rise in temperature was detected. The RCPD irradiated at 0.3 W/cm^2 showed a temperature increase of only 10.0°C, exhibited no PTT effect (Figure 2F). Thus, by varying laser power density, therapeutic application of RCPD could be tuned from PDT to combinatorial PDT–PTT treatment. Overall, these results suggested that RCPD had an excellent potential to act as a synergistic phototherapy nanoplatform with double tunable PDT and PTT properties. Hence, RCPD at a concentration of 0.16 mM (cypate-equiv) and irradiated with a portable laser at 1.6 W/cm^2 for 5 mins could completely ablate the tumor.

Cell uptake and internalization of RCPD

The cellular uptake and internalization of RCPD in αvβ3-positive HepG2 cells was studied by confocal microscopy. As shown in Figure 3A, green image shows cell lysosome stained with lysotracker green and red image shows cypate fluorescence in RCPD. RCPD were internalized into cells after 1 hr post-incubation, and fluorescence intensity reached a maximum for 2 hrs incubation, and then gradually diminished over time (Figure 3B). Hence, we chose to irradiate the cells with NIR laser after incubation for 2 hrs with RCPD. These results indicated that RCPD could be efficiently taken up by cancer cells and escaped from lysosome to kill cancer cells.

Intracellular generation of ROS and heat

The level of intracellular ROS generation of RCPD in HepG2 cells upon NIR irradiation was assessed using a ROS-detecting fluorescent probe (DCFH-DA). As expected, RCPD-treated cancer cells exposed to NIR light (808 nm, 1.6 W/cm^2, 5 mins) exhibited stronger fluorescence intensity than cypate-treated cancer cells because of the reduction of aggregation in cypate, indicative of a high level of intracellular ROS generation (Figure 4A). No ROS was generated in the control group and RCPD-treated cells in absence of NIR irradiation. A flow cytometry analysis further confirmed the significant increase of ROS generation in RCPD-treated cancer cells compared with free cypate (Figure 4B). The generation of ROS was accompanied by an increase of temperature in RCPD (increase to 44.7°C) or free cypate (increase to 44.4°C) treated cells. However, the temperature in free cypate-treated cells cannot be maintained for a long time (Figure 4C). This may be due to the photobleaching of cypate, and the results were consistent with the in vitro data. These in vitro cell studies demonstrated that RCPD could kill cancer cells through the combined effects of intracellular generation of ROS and hyperthermia.

In vitro combination therapeutic efficacy of RCPD

Synergistic cytotoxicity of RCPD-mediated combination treatment of PTT/PDT and chemotherapy were assessed in HepG2 cells and DTX-resistant human liver cancer cells

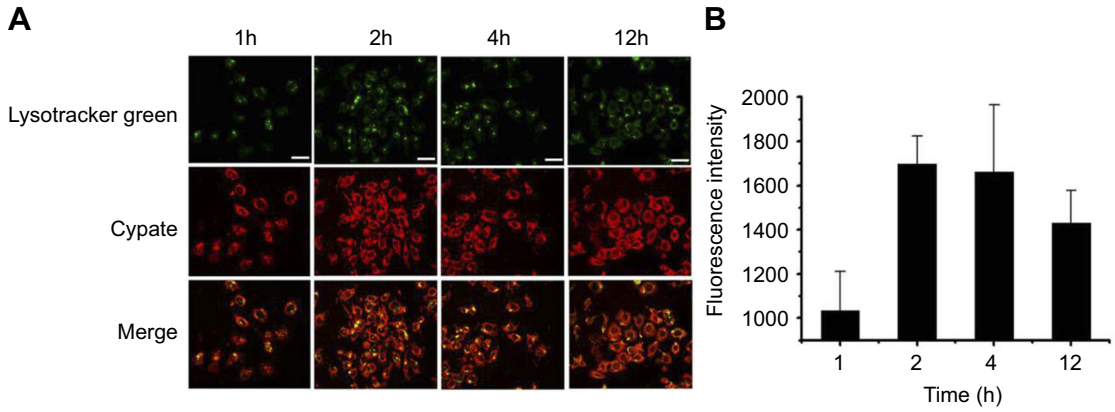

Figure 3 (**A**) Confocal images of HepG2 cells after 1 hr, 2 hrs, 4 hrs, and 12 hrs of incubation with RCPD. Scale bar is 40 μm. (**B**) The confocal microscopy analysis of cellular uptakes of RCPD at different time.

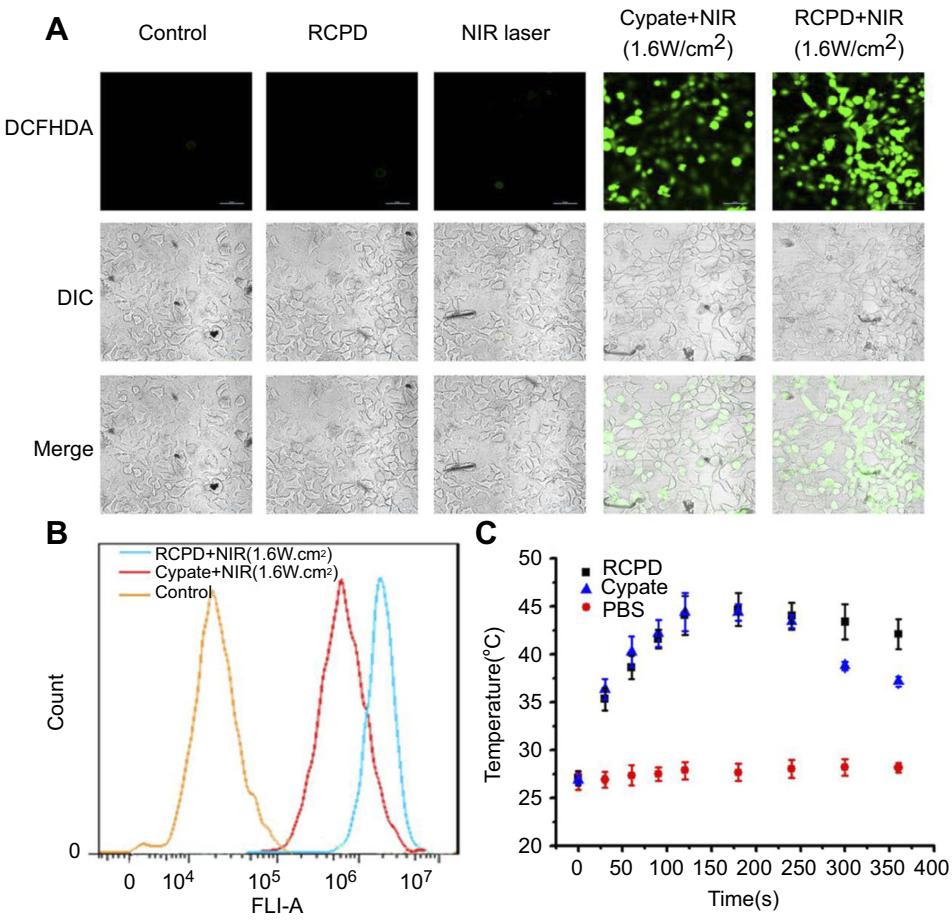

Figure 4 (**A**) Confocal images of ROS generation in HepG2 cells at 24 hrs after various treatments. Scale bar is 50 μm. (**B**) The flow cytometric analysis of intracellular ROS productions in HepG2 cells treated with RCPD or cypate after NIR irradiation (1.6 W/cm^2, 5 mins). (**C**) Temperature viabilities of HepG2 cells treated with PBS, RCPD, or cypate.
Abbreviations: ROS, reactive oxygen species.

by performing MTT assay. In our previous study, RCP had no significant cytotoxicity at different concentrations (0.1, 1, 10, 100, and 1000 μM) used in cell experiments.[46] As shown in Figure S4, cell viability of RCPD at 31 μg/mL (2.3 μM DTX-equiv.) was 54.05% and 45.07% after 24 hrs and 48 hrs, which reduced to 35.54% and 23.52% at 500 μg/mL (37.2 μM DTX-equiv.) separately. As expected, the growth inhibition effect was enhanced as the drug loading concentrations increased. Furthermore, the cell viabilities of RCPD in DTX-resistant HepG2 cells were higher than the normal HepG2 cells at the same concentration for both 24 hrs and 48 hrs. Then we tested the therapeutic effect of RCPD upon laser irradiation in DTX-resistant HepG2 cells and the results were shown in Figure 5B. Specifically, NIR laser irradiation at power densities of 1.6 W/cm^2 had no obvious influence on cell growth at 24 hrs.[49] The laser power density of 0.3 W/cm^2 was specifically chosen based on our solution studies (Figure 2F) to evaluate only the photodynamic effect of RCPD. The cytotoxicity of RCPD with PDT (16.84%) was nearly identical to that of free DTX (18.51%). In addition, the cytotoxicity of RCP with PDT and PTT (phototherapy only, 808 nm, exposed to 1.6 W/cm^2 NIR laser, 11.51%) was higher than RCPD with PDT, which was probably due to the fact that PTT was more lethal than chemotherapy alone. Remarkably, RCPD with PDT and PTT (808 nm, exposed to 1.6 W/cm^2 light, 6.62%) exhibited significantly stronger cytotoxicity than any other treatments. which indicated the sensitivity of DTX-resistant HepG2 cells to PDT and hyperthermia.[50] Therefore, the combined chemo-phototherapy could be an efficient approach for treatment of multidrug-resistant cancer cells.

To visually evaluate the combination treatment effect, DTX-resistant HepG2 cells with various treatments were further tested by the LIVE/DEAD Kit, in which Calcein-AM and PI were used to stain the live and dead cells with green and red fluorescence. The images of cells after treatments are shown in Figure 5A. Weak red fluorescence

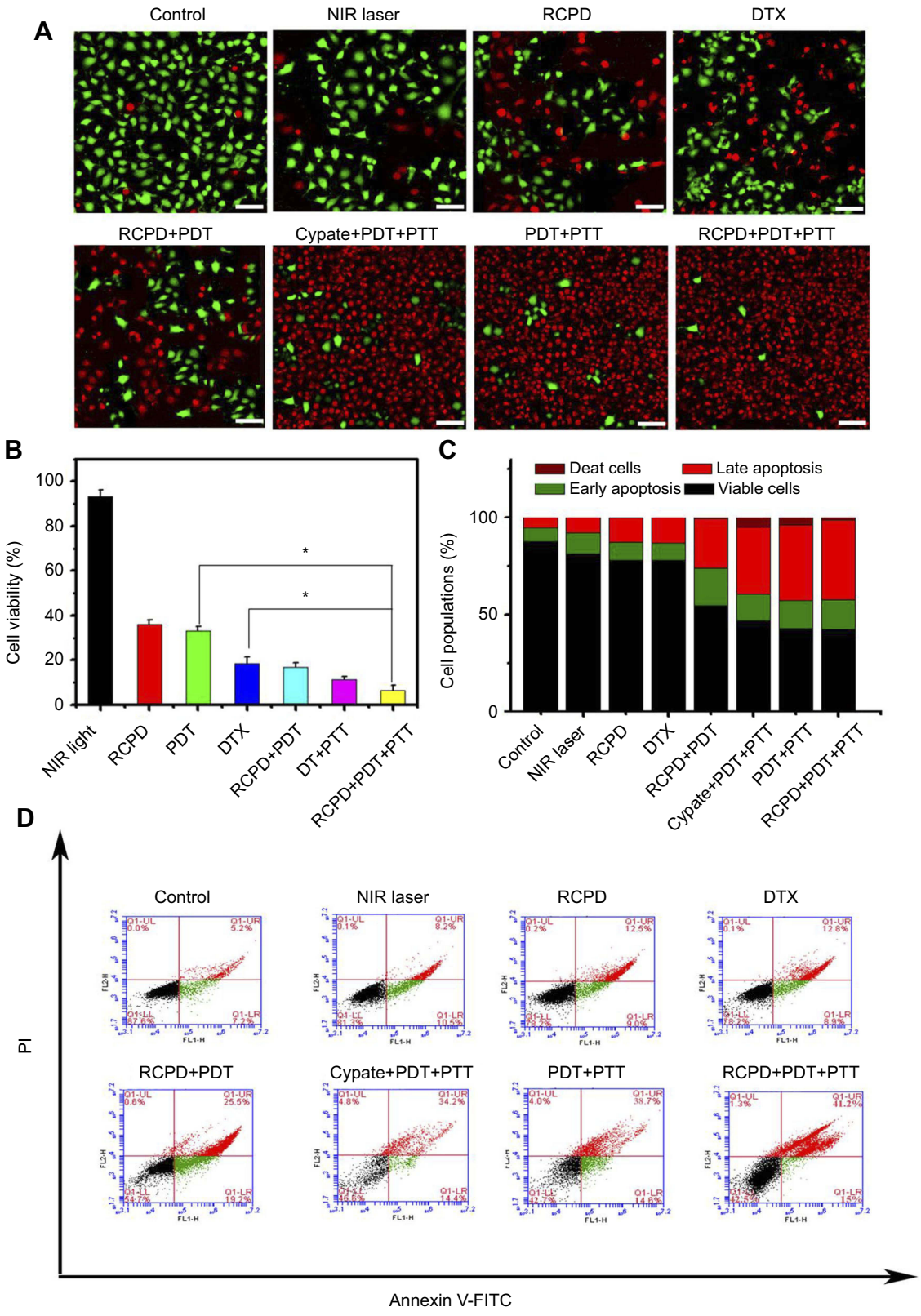

Figure 5 (**A**) The LIVE-DEAD analysis of HepG2 cells at 24 hrs after various treatments. Scale bar is 100 μm. (**B**) The cell viability of DTX-resistant human liver cancer cells at 24 hrs after various treatments (*p<0.05). (**C**) Stacked bars of HepG2 cells apoptosis determined by flow cytometry using Annexin V-FITC and PI. (**D**) The cell apoptosis quantified by the flow cytometry at 24 hrs after various treatments. The cypate and DTX concentrations were 32 μM and 18.6 μM, respectively. In all experiments, PDT was irradiated with 808 nm, 0.3 W/cm^2, PDT+PTT was irradiated with 808 nm, 1.6 W/cm^2.

Abbreviations: PTT, photothermal therapy; PDT, photodynamic therapy.

and strong green fluorescence was observed in the cells treated with PBS and NIR light, and red fluorescent signals were clearly visible in the cells treated with RCPD, free DTX, RCPD (0.3 W/cm^2), cypate (1.6 W/cm^2), and RCP (1.6 W/cm^2), and fluorescence intensity in these groups are gradually enhanced. Remarkably, cells treated with RCPD (1.6 W/cm^2) almost entirely died. The results suggested that chemotherapy combined with phototherapy (PDT +PTT) performed the strongest ability to kill tumor cells, while RCPD, free DTX, cypate, RCPD with PDT and phototherapy (PDT+PTT) alone could only kill cells partially; PBS and NIR light had no significant cytotoxicity on cells.

Apoptosis of HepG2 cells was detected by flow cytometry to further quantitatively analyze the antitumor effects in different treatment conditions and investigate anti-tumor mechanisms. As shown in Figure 5C and D, the percentage of viable cells of both control (87.6%) and NIR laser group (1.6 W/cm^2, 81.3%) were much higher than that of RCPD-treated cells. The percentage of apoptotic cells and necrotic/dead cells followed the order: RCPD (21.5%) < DTX (21.7%) < RCPD (0.3 W/cm^2, 44.7%) < cypate (1.6 W/cm^2, 48.6%) < RCP (1.6 W/cm^2, 53.3%) and < RCPD (1.6 W/cm^2, 56.2%). This result was consistent with the Calcein-AM/PI kit result.

The above results clearly testified that RCPD could generate both $^1O_2$ and heat inside cells upon exposure to NIR, confirming the activation of PDT and PTT mechanism. Moreover, the therapeutic mechanism can be switched from PDT only (0.3 W/cm^2) to combinatorial phototherapy (1.6 W/cm^2) by changing the laser power. Synergistic therapeutic results indicated combined chemo-photo therapy was more cytotoxic to cancer cells than phototherapy or chemotherapy alone. Moreover, RCPD with PDT and PTT (1.6 W/cm^2) had a good effect on solving multi-drug resistance owing to the auxiliary role of phototherapy. Moreover, combination treatment of chemotherapy and phototherapy (PDT+PTT) had higher apoptosis and necrotic rate than any other treatment, indicating RCPD exposed to NIR laser could directly kill tumor cells by activating the apoptotic pathway.

In vivo tumor-targeting and synergistic chemo-photo therapeutic efficacy

Biodistribution and in vivo tumor-targeting ability were investigated by NIR imaging system. Cypate-PAMAM (CP) or RCP (0.5 mg/kg equivalent to cypate) was administered via the tail vein to HepG2 tumor-bearing mice. Figure S5 showed that only a weak fluorescence signal was observed in the tumor region in mice treated with CP. In contrast, RCP exhibited much higher fluorescence signal in the tumor region after 4 hrs post-injection and the fluorescence intensity gradually increased with time prolonged and maintained up to 24 hrs, demonstrating RCP could preferentially localize at tumor sites through EPR effect and active targeting mediated by iRGD.

With tumor uptake of RCP having been demonstrated, we further assessed PTT/PDT efficacy of RCPD in HepG2 tumor-bearing mice. SOSG was used as a fluorescence probe for detecting intratumoral $^1O_2$ production. Confocal images of SOSG-stained tumor sections are shown in Figure 6A; tumors treated with NIR laser, DTX, and RCPD without NIR irradiation exhibited almost no green

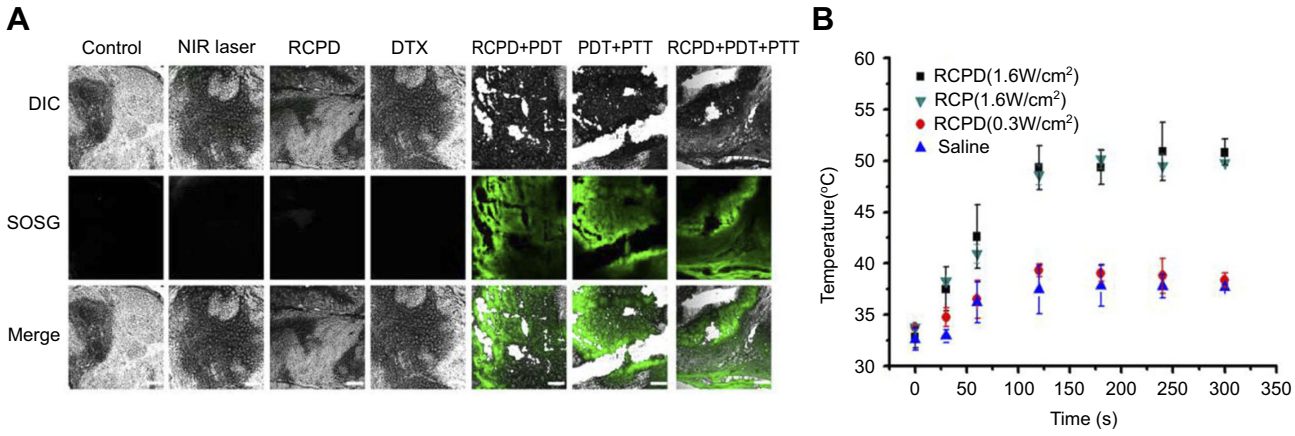

Figure 6 (**A**) The confocal images of SOSG-stained sections at 6 hrs after various treatments. Scale bars represent 100 μm. (**B**) Temperature change curves in tumors exposed to the 808 nm laser at a power density of 0.3 W/cm^2 and 1.6 W/cm^2 after intravenous injections of saline, RCP, and RCPD.
Abbreviations: SOSG, singlet oxygen sensor green.

fluorescence signals. However, after laser irradiation, the tumors showed strong green fluorescence signals at 6 hrs post-injections of RCP and RCP. These results demonstrated that RCP and RCPD with NIR laser can trigger the generation of large amounts of $^1O_2$. For the changes of tumor temperature, RCP and RCPD with laser irradiation (1.6 W/cm^2) can quickly increase tumor temperature to 50° C, which was sufficient for tumor ablation. However, RCPD with laser irradiation (0.3 W/cm^2) can only increase tumor temperature to about 38.4°C, which had same effect compared with PBS, as shown in Figure 6B. All these results suggested that RCPD with laser irradiation (1.6 W/cm^2) had strong in vivo PDT/PTT efficacy.

Therapeutic efficacy following intravenous injection and subsequent NIR irradiation was evaluated by measuring tumor volume and bodyweight. We found that no obvious inhibition of tumor growth was observed in saline alone or saline + NIR (1.6 W/cm^2) groups, and tumor volumes in these two groups were similar (Figure 7A). All other treatments significantly inhibited the tumor growth. Compared to free DTX, RCPD had a higher inhibitory effect due to their good tumor-retention

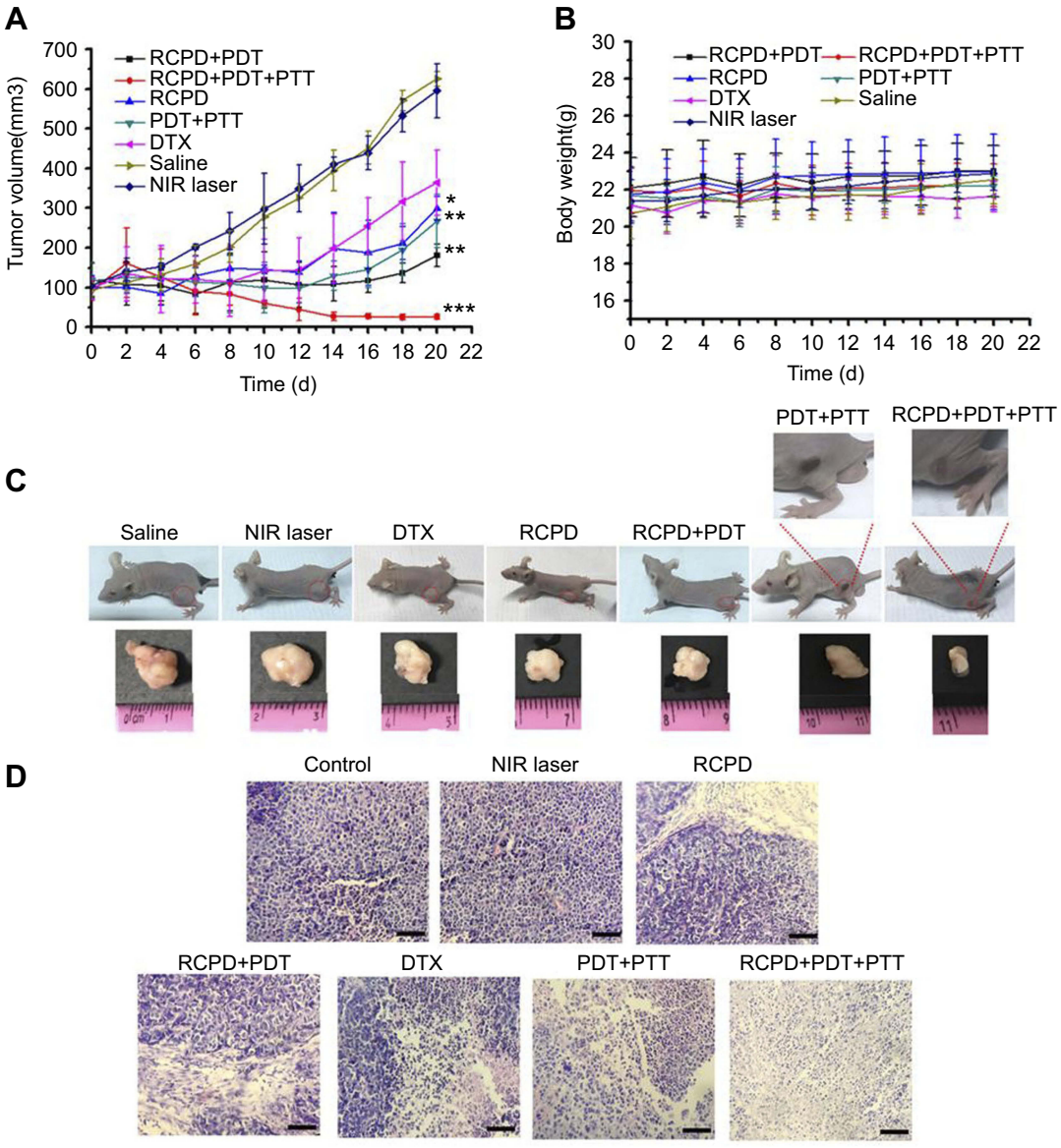

Figure 7 (**A**) The tumor growth curves of mice after various treatments. (**B**) The body weight changes of mice during various treatments. (**C**) The photos of mice and excised tumors after various treatments. The red circles indicate the tumor size. (**D**) The images of H&E stained tumor sections after various treatments. Scale bars represent 50 μm. The doses of cypate and DTX in all the above experiments were 6.7 and 5 mg/kg. The laser irradiation was carried out on the tumor at 808 nm at a power density of 0.3 W/cm^2 or 1.6 W/cm^2 for 5 mins. -*p<0.05, **p<0.01, ***p<0.001 for comparison to the control-.

capability. During the first 10 days, tumors with treatments of PDT+PTT (RCP+1.6W/cm^2), RCPD+PDT (RCPD +0.3W/cm^2), and RCPD+PDT+PTT (RCPD+1.6W/cm^2) were significantly inhibited after laser irradiation. But unfortunately, the tumors treated with PDT+PTT (RCP +1.6W/cm^2), RCPD+PDT (RCPD+0.3W/cm^2) rapidly recurred afterward, indicating that there were some tumor cells survived from PTT/PDT treatment. Low generation of singlet oxygen due to severe hypoxia in tumor center and limited diffusion distance of ROS produced by PDT in cytoplasm greatly limit the therapeutic effect, hence phototherapy alone easily caused tumor recurrence.[51–53] However, the recurrence rate of RCPD+PDT (RCPD +0.3W/cm^2) was much lower than that of PDT+PTT (RCP+1.6W/cm^2), which should be attributed to the chemotherapy efficacy of RCPD. Moreover, RCPD+PDT +PTT (RCPD+1.6W/cm^2) mediated combination treatment of PTT/PDT and chemotherapy showed the most potent antitumor efficacy and almost no tumor recurred in the treated mice until 20 d thereafter.

The body weights of mice were measured at time intervals after initial treatments. The results demonstrated that RCPD+PDT+PTT exerted photo-chemotherapeutic synergistic efficacy. As shown in Figure 7B, all mice displayed no obvious decreases in body weights, suggesting the high biosafety of these treatments. The photos of mice with these treatments are shown in Figure 7C. The burn scars were clearly observed in mice at 20 d after treatments. After laser irradiation, tumors treated with PDT+PTT recurred obviously at the edge of laser spot at 11 d and gradually grew to large sizes after the last treatment. To further evaluate treatment effect induced by these treatments, tumor sections were stained with H&E for histopathological observation. As shown in Figure 7D, nuclear pyknosis and nuclear fragmentation were observed in tumors treated with free DTX and RCPD, and furthermore, nuclear lysis and tumor necrosis were visible in tumors with treatments of PDT+PTT, RCPD+PDT and RCPD+PDT+PTT after laser irradiation. These results demonstrated that RCPD+PDT+PTT could effectively ablate tumor and prevent tumor recurrence.

Phototherapy can directly kill tumor cells as a local treatment modality. However, tumor cells that survived from PDT can result in regrowth of tumor cells and tumor vessels. Chemotherapy can further damage tumor cells and prevent their regrowth.[9] Therefore, RCPD exposed to NIR light could combine phototherapy and chemotherapy together to be a more effective systemic anti-cancer treatment option. Such combination treatments have been tested clinically and demonstrated an enhanced anti-tumor response compared to either phototherapy or chemotherapy alone.[54,55]

Conclusion

In conclusion, iRGD-cypate-PAMAM-DTX (RCPD) is a new multifunctional nanoplatform to facilitate cancer treatment and reduce the risk of recurrence by combining chemo-phototherapy of cancer cells. The presented results indicated that RCPD had strong in vitro and in vivo PTT/PDT efficacy and could transform PDT to combinatorial PDT–PTT treatment by varying laser power density. Furthermore, in vitro cell studies demonstrated that RCPD displayed a potential to reverse overcome multidrug resistance in HepG2 cancer cells, with more nanoparticles transport into the tumor cells. In vivo antitumor studies demonstrated that compared with phototherapy alone, the combined chemo-phototherapy treatment could significantly reduce the risk of recurrence and enhance anti-tumor efficiency.[37–41,55] All the experimental results proved that the combination of phototherapy and chemotherapy of RCPD is an effective approach to achieve excellent therapeutic effect of tumors. We propose that our nanoplatform can be a promising strategy for cancer therapy with a great potential for clinical application.

Abbreviation list

iRG, DCRGDKGPDC; DTX, Docetaxel; PAMAM, polyamindoamine; CP, Cypate-PAMAM; RCP, iRGD-cypate-PAMAM; RCPD, iRGD-Cypate-PAMAM-DTX; DMF N, N-Dimcthylformamide; EDCI, 1-ethyl-3-(3′-dimethylaminopropyl) carbodiimide; NHS, N-hydroxysuccinimide; DPBF, 1, 3-Diphenylisobenzofuran; FBS, Fetal bovine serum; DLS, Dynamic light scattering; TEM, Transmission electron microscopy; DCFH-DA, 2′,7′-dichlorofluorescin diacetate; MTT, Methyl thiazolyltetrazolium.

Acknowledgments

This work was financially supported by the National Natural Science Foundation of China (No. 81673360 and 81601591), Shandong Provincial Natural Science Foundation (No. ZR2016HM45, ZR2017BH006 and ZR2016HB15), China Postdoctoral Natural Science Foundation (2017M612210), and Scientific Research Foundation for Youth Scholars from Qingdao University (No. 41117010026). The authors would like to thank Mr. Qingming Ma for his writing assistance.

Disclosure

The authors report no conflicts of interest in this work.

References

1. Chatterjee DK, Fong LS, Zhang Y. Nanoparticles in photodynamic therapy: an emerging paradigm. *Adv Drug Deliv Rev*. 2008;60(15):1627–1637. doi:10.1016/j.addr.2008.08.003
2. Cherukula K, Lekshmi KM, Uthaman S, Cho K, Cho CS, Park IK. Multifunctional inorganic nanoparticles: recent progress in thermal therapy and imaging. *Nanomaterials*. 2016;6(4):76. doi:10.3390/nano6040076
3. Huang X, Zhang W, Guan G, Song G, Zou R, Hu J. Design and functionalization of the NIR-responsive photothermal semiconductor nanomaterials for cancer theranostics. *Acc Chem Res*. 2017;50(10):2529–2538. doi:10.1021/acs.accounts.7b00294
4. Lucky SS, Soo KC, Zhang Y. Nanoparticles in photodynamic therapy. *Chem Rev*. 2015;115(4):1990–2042. doi:10.1021/cr5004198
5. Song X, Chen Q, Liu Z. Recent advances in the development of organic photothermal nano-agents. *Nano Res*. 2015;8(2):340–354. doi:10.1007/s12274-014-0620-y
6. Zhou Z, Kong B, Yu C, et al. Tungsten oxide nanorods: an efficient nanoplatform for tumor CT imaging and photothermal therapy. *Sci Rep*. 2014;4(1):3653. doi:10.1038/srep03653
7. Agostinis P, Berg K, Cengel KA, et al. Photodynamic therapy of cancer: an update. *CA Cancer J Clin*. 2011;61(4):250–281. doi:10.3322/caac.20114
8. Li YB, Lu W, Huang QA, Huang MA, Li C, Chen W. Copper sulfide nanoparticles for photothermal ablation of tumor cells. *Nanomedicine*. 2010;5(8):1161−1171. doi:10.2217/nnm.10.2
9. Luo D, Carter KA, Miranda D, Lovell JF. Chemophototherapy: an emerging treatment option for solid tumors. *Adv Sci*. 2017;4(1):1600106. doi:10.1002/advs.201600106
10. Li LB, Xie JM, Zhang XN, et al. Retrospective study of photodynamic therapy vs photodynamic therapy combined with chemotherapy and chemotherapy alone on advanced esophageal cancer. *Photodiagn Photodyn Ther*. 2010;7(3):139–143. doi:10.1016/j.pdpdt.2010.06.002
11. Zou L, Wang H, He B, et al. Current approaches of photothermal therapy in treating cancer metastasis with nanotherapeutics. *Theranostics*. 2016;6(6):762–772. doi:10.7150/thno.14988
12. Cao J, Chen Z, Chi J, Sun Y, Sun Y. Recent progress in synergistic chemotherapy and phototherapy by targeted drug delivery systems for cancer treatment. *Artif Cells Nanomed Biotechnol*. 2018;46(Suppl 1):817–830. doi:10.1080/21691401.2018.1436553
13. Postiglione I, Chiaviello A, Palumbo G. Enhancing photodynamyc therapy efficacy by combination therapy: dated, current and oncoming strategies. *Cancers*. 2011;3(2):2597–2629. doi:10.3390/cancers3022597
14. Qin SY, Cheng YJ, Lei Q, Zhang AQ, Zhang XZ. Combinational strategy for high-performance cancer chemotherapy. *Biomaterials*. 2018;171:178–197. doi:10.1016/j.biomaterials.2018.04.027
15. Carter KA, Luo D, Razi A, et al. Sphingomyelin liposomes containing porphyrin-phospholipid for irinotecan chemophototherapy. *Theranostics*. 2016;6(13):2329–2336. doi:10.7150/thno.15701
16. Choi JY, Thapa RK, Yong CS, Kim JO. Nanoparticle-based combination drug delivery systems for synergistic cancer treatment. *J Pharm Invest*. 2016;46(4):325–339. doi:10.1007/s40005-016-0252-1
17. Jiao L, Jie C, Jianhua C, et al. Mechanistic insight into the interaction of gastrointestinal mucus with oral diblock copolymers synthesized via ATRP method. *Int J Nanomedicine*. 2018;13:2839–2856. doi:10.2147/IJN.S160651
18. Liu B, Li C, Chen G, et al. Synthesis and optimization of MoS2@Fe3O4-ICG/Pt(IV) nanoflowers for MR/IR/PA bioimaging and combined PTT/PDT/chemotherapy triggered by 808 nm laser. *Adv Sci*. 2017;4(8):1600540. doi:10.1002/advs.201600540
19. Jiang L, Liang Y, Huo Q, et al. Viral capsids mimicking based on pH-sensitive biodegradable polymeric micelles for efficient anticancer drug delivery. *J Biomed Nanotechnol*. 2018;14(8):1409–1419. doi:10.1166/jbn.2018.2587
20. Liu Y, Jiang Y, Zhang M, Tang Z, He M, Bu W. Modulating hypoxia via nanomaterials chemistry for efficient treatment of solid tumors. *Acc Chem Res*. 2018;51(10):2502–2511. doi:10.1021/acs.accounts.8b00214
21. Tang J, Zhou H, Hou X, et al. Enhanced anti-tumor efficacy of temozolomide-loaded carboxylated poly(amido-amine) combined with photothermal/photodynamic therapy for melanoma treatment. *Cancer Lett*. 2018;423:16–26. doi:10.1016/j.canlet.2018.03.002
22. Wang N, Feng Y, Zeng L, Zhao Z, Chen T. Functionalized multi-walled carbon nanotubes as carriers of ruthenium complexes to antagonize cancer multidrug resistance and radioresistance. *ACS Appl Mater Interfaces*. 2015;7(27):14933–14945. doi:10.1021/acsami.5b03739
23. Wang X, Ma Y, Chen H, et al. Novel doxorubicin loaded PEGylated cuprous telluride nanocrystals for combined photothermal-chemo cancer treatment. *Colloids Surf B Biointerfaces*. 2017;152:449–458. doi:10.1016/j.colsurfb.2017.02.002
24. Zhan Q, Qian J, Liang H, et al. Using 915 nm laser excited Tm3+/Er3+/Ho3+-Doped NaYbF4 upconversion nanoparticles for *in vitro* and deeper *in vivo* bioimaging without overheating irradiation. *ACS Nano*. 2011;5(5):3744–3757. doi:10.1021/nn200110j
25. Fan W, Huang P, Chen X. Overcoming the Achilles' heel of photodynamic therapy. *Chem Soc Rev*. 2016;45(23):6488–6519. doi:10.1039/c6cs00616g
26. Pansare VJ, Hejazi S, Faenza WJ, Prud'homme RK. Review of long-wavelength optical and NIR imaging materials: contrast agents, fluorophores, and multifunctional nano carriers. *Chem Mater*. 2012;24(5):812–827. doi:10.1021/cm2028367
27. Feng Q, Zhang Y, Zhang W, et al. Programmed near-infrared light-responsive drug delivery system for combined magnetic tumor-targeting magnetic resonance imaging and chemo-phototherapy. *Acta Biomater*. 2017;49:402–413. doi:10.1016/j.actbio.2016.11.035
28. Gong H, Cheng L, Xiang J, et al. Near-infrared absorbing polymeric nanoparticles as a versatile drug carrier for cancer combination therapy. *Adv Funct Mater*. 2013;23(48):6059–6067. doi:10.1002/adfm.201301555
29. Park H, Kim J, Jung S, Kim WJ. DNA-Au nanomachine equipped with i-Motif and G-quadruplex for triple combinatorial anti-tumor therapy. *Adv Funct Mater*. 2018;28(5):1705416. doi:10.1002/adfm.v28.5
30. Cao J, Chen D, Huang SS, Deng DW, Tang L, Gu YQ. Multifunctional near-infrared light-triggered biodegradable micelles for chemo- and photo-thermal combination therapy. *Oncotarget*. 2016;7:82170–82184. doi:10.18632/oncotarget.10320
31. Chen Q, Liang C, Wang C, Liu Z. An imagable and photothermal "Abraxane-like" nanodrug for combination cancer therapy to treat subcutaneous and metastatic breast tumors. *Adv Mater*. 2015;27(5):903–910. doi:10.1002/adma.201404308
32. Li Q, Li W, Di H, et al. A photosensitive liposome with NIR light triggered doxorubicin release as a combined photodynamic-chemo therapy system. *J Control Release*. 2018;277:114–125. doi:10.1016/j.jconrel.2018.02.001
33. Lin L, Liang X, Xu Y, Yang Y, Li X, Dai Z. Doxorubicin and indocyanine green loaded hybrid bicelles for fluorescence imaging guided synergetic chemo/photothermal therapy. *Bioconjug Chem*. 2017;28(9):2410–2419. doi:10.1021/acs.bioconjchem.7b00407

34. Liu X, Wang Y, Yu Q, et al. Selenium nanocomposites as multifunctional nanoplatform for imaging guiding synergistic chemo-photothermal therapy. *Colloids Surf B Biointerfaces*. 2018;166:161–169. doi:10.1016/j.colsurfb.2018.03.018
35. Zhang M, Zhang L, Chen Y, Li L, Su Z, Wang C. Precise synthesis of unique polydopamine/mesoporous calcium phosphate hollow Janus nanoparticles for imaging-guided chemo-photothermal synergistic therapy. *Chem Sci*. 2017;8(12):8067–8077. doi:10.1039/c7sc03521g
36. Zhao J, Wan Z, Zhou C, et al. Hyaluronic acid Layer-By-Layer (LbL) nanoparticles for synergistic chemo-phototherapy. *Pharm Res*. 2018;35(10):196. doi:10.1007/s11095-018-2480-8
37. Guo Y, Jiang K, Shen Z, et al. A small molecule nanodrug by self-assembly of dual anticancer drugs and photosensitizer for synergistic near-infrared cancer theranostics. *ACS Appl Mater Interfaces*. 2017;9(50):43508–43519. doi:10.1021/acsami.7b14755
38. Li X, Zhao X, Pardhi D, et al. Folic acid modified cell membrane capsules encapsulating doxorubicin and indocyanine green for highly effective combinational therapy *in vivo*. *Acta Biomater*. 2018;74:374–384. doi:10.1016/j.actbio.2018.05.006
39. Shu Y, Song R, Zheng A, Huang J, Chen M, Wang J. Thermo/pH dual-stimuli-responsive drug delivery for chemo-/photothermal therapy monitored by cell imaging. *Talanta*. 2018;181:278–285. doi:10.1016/j.talanta.2018.01.018
40. Vivek R, Varukattu N, Chandrababu R, et al. Multifunctional nanoparticles for trimodal photodynamic therapy-mediated photothermal and chemotherapeutic effects. *Photodiagnosis Photodyn Ther*. 2018;23:244–253. doi:10.1016/j.pdpdt.2018.06.025
41. Wan G, Chen B, Li L, et al. Nanoscaled red blood cells facilitate breast cancer treatment by combining photothermal/photodynamic therapy and chemotherapy. *Biomaterials*. 2018;155:25–40. doi:10.1016/j.biomaterials.2017.11.002
42. Tan X, Wang J, Pang X, et al. Indocyanine green-loaded silver nanoparticle@polyaniline core/shell theranostic nanocomposites for photoacoustic/near-infrared fluorescence imaging-guided and single-light-triggered photothermal and photodynamic therapy. *ACS Appl Mater Interfaces*. 2016;8(51):34991–35003. doi:10.1021/acsami.6b11262
43. Tran TH, Nguyen HT, Le NV, et al. Engineering of multifunctional temperature-sensitive liposomes for synergistic photothermal, photodynamic, and chemotherapeutic effects. *Int J Pharm*. 2017;528(1–2):692–704. doi:10.1016/j.ijpharm.2017.06.069
44. Zhang X, Luo L, Li L, et al. Trimodal synergistic antitumor drug delivery system based on graphene oxide. *Nanomedicine*. Epub 2018 Sep 24.
45. Miao W, Kim H, Gujrati V, et al. Photo-decomposable organic nanoparticles for combined tumor optical imaging and multiple phototherapies. *Theranostics*. 2016;6(13):2367–2379. doi:10.7150/thno.15829
46. Cao J, Ge R, Zhang M, et al. A triple modality BSA-coated dendritic nanoplatform for NIR imaging, enhanced tumor penetration and anticancer therapy. *Nanoscale*. 2018;10(19):9021–9037. doi:10.1039/c7nr09552j
47. Spiller W, Kliesch H, Wöhrle D, Hackbarth S, Röder B, Schnurpfeil G. Singlet oxygen quantum yields of different photosensitizers in polar solvents and micellar solutions. *J Porphyr Phthalocyanines*. 1998;2(2):145–158. doi:10.1002/(SICI)1099-1409(199803/04)2:2<145::AID-JPP60>3.0.CO;2-2
48. Cardillo JA, Jorge R, Costa RA, et al. Experimental selective choriocapillaris photothrombosis using a modified indocyanine green formulation. *Br J Ophthalmol*. 2008;92(2):276–280. doi:10.1136/bjo.2007.129395
49. Zhu L, Wang C, Pang DW, Zhang ZL. Controlled release of therapeutic agents with near-infrared laser for synergistic photochemotherapy toward cervical cancer. *Anal Chem*. 2019. doi:10.1021/acs.analchem.8b05982
50. Taratula O, Schumann C, Duong T, Taylor KL. Dendrimer-encapsulated naphthalocyanine as a single agent-based theranostic nanoplatform for near-infrared fluorescence imaging and combinatorial anticancer phototherapy. *Nanoscale*. 2015;7(9):3888–3902. doi:10.1039/c4nr06050d
51. Wang W, Moriyama LT, Bagnato VS. Photodynamic therapy induced vascular damage: an overview of experimental PDT. *Laser Phys Lett*. 2013;10(2):023001. doi:10.1088/1612-2011/10/2/023001
52. Sitnik TM, Hampton JA, Henderson BW. Reduction of tumour oxygenation during and after photodynamic therapy *in vivo*: effects of fluence rate. *Br J Cancer*. 1998;77(9):1386–1394. doi:10.1038/bjc.1998.231
53. Liu J, Liang H, Li M, et al. Tumor acidity activating multifunctional nanoplatform for NIR-mediated multiple enhanced photodynamic and photothermal tumor therapy. *Biomaterials*. 2018;157:107–124. doi:10.1016/j.biomaterials.2017.12.003
54. Jin ML, Yang BQ, Zhang W, et al. Combined treatment with photodynamic therapy and chemotherapy for advanced cardiac cancers. *J Photochem Photobiol B*. 1992;12(1):101–106.
55. Hong MJ, Cheon YK, Lee EJ, et al. Long-term outcome of photodynamic therapy with systemic chemotherapy compared to photodynamic therapy alone in patients with advanced hilar cholangiocarcinoma. *Gut Liver*. 2014;8(3):318–323. doi:10.5009/gnl.2014.8.3.318

Supplementary materials

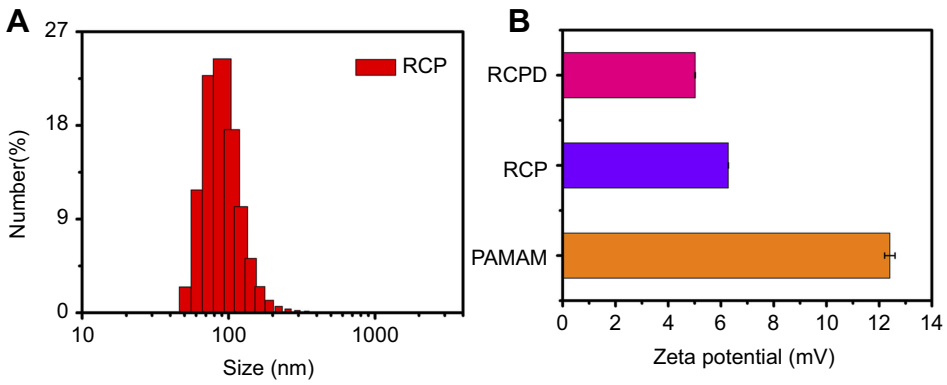

Figure S1 (**A**) Size distribution of RCP (**B**) Zeta potential of RCPD, RCP and PAMAM.

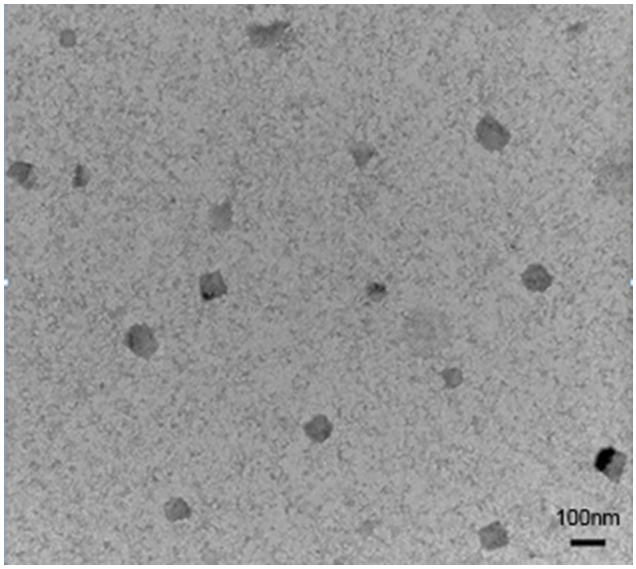

Figure S2 TEM image of RCPD. Scale bar is 100nm.

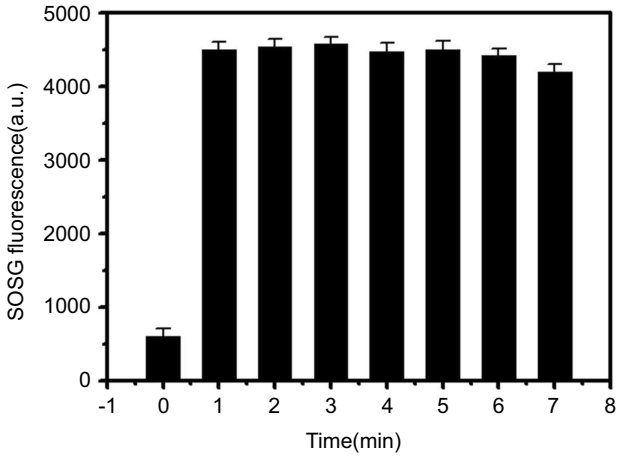

Figure S3 Singlet oxygen generation at different time by RCPD (0.16 mM cypate-equiv) after NIR irradiation (808 nm laser diode, 1.6 W/cm^2).

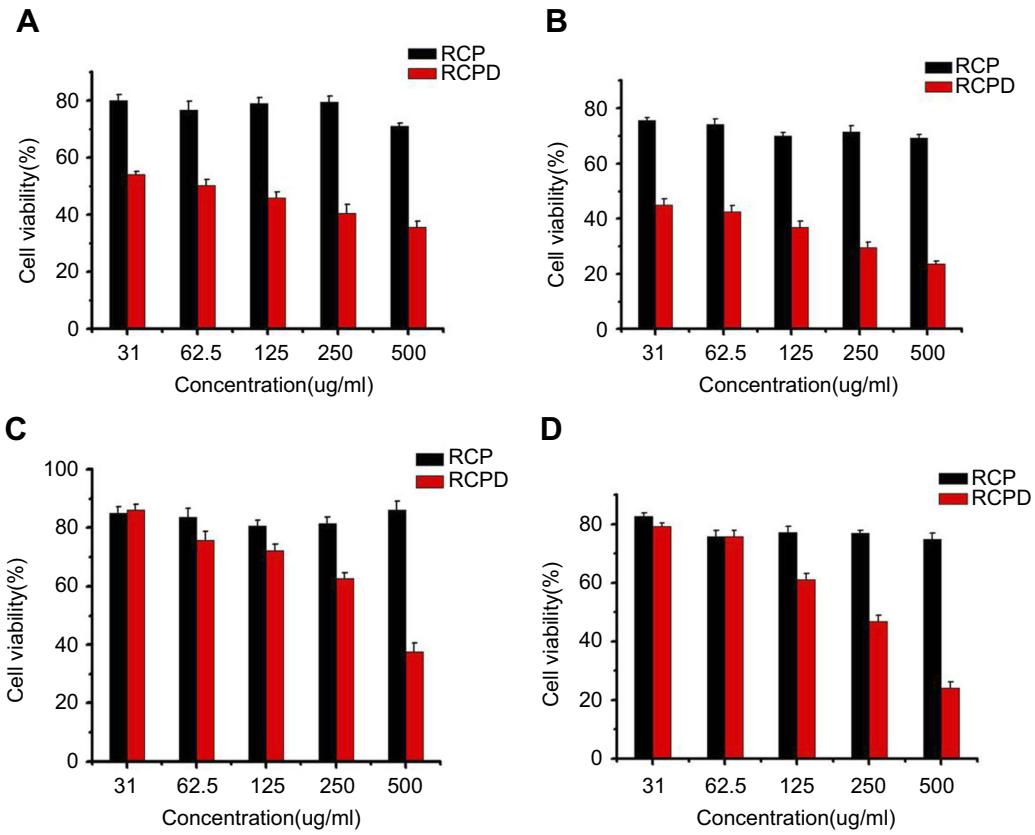

Figure S4 Cytotoxicity on HepG2 cells incubated with different concentrations of RCP or RCPD at (**A**) 24 h, (**B**) 48 h. Cytotoxicity on Paclitaxel resistant HepG2 cells incubated with different concentrations of RCP or RCPD at (**C**) 24h, (**D**) 48h. The doses of DTX in all above experiments was 2.3-37.2 μM.

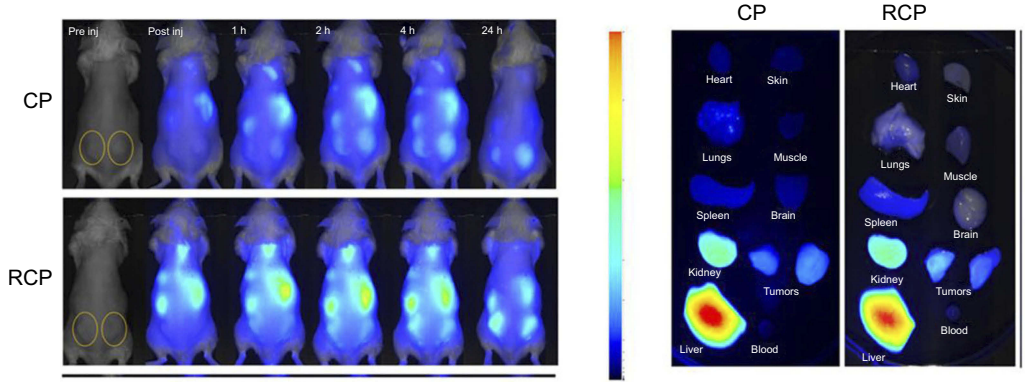

Figure S5 NIR images of HepG2 tumor xenograft bearing nude mice after intravenous injection CP or RCP and main organs excised from the tumor mice 24 h after intravenous injection of CP or RCP.